Journal of Materials Chemistry C

PAPER

View Article Online
View Journal

Cite this: DOI: 10.1039/c8tc05764h

Vinylene-bridged difluorobenzo[*c*][1,2,5]-thiadiazole (FBTzE): a new electron-deficient building block for high-performance semiconducting polymers in organic electronics†

Yuya Asanuma,[a] Hiroki Mori,[b] Ryosuke Takahashi[a] and Yasushi Nishihara *[b]

A new class of an acceptor unit, vinylene-bridged 5,6-difluorobenzothiadiazole **FBTzE**, has been developed. Palladium-catalyzed Migita–Kosugi–Stille coupling reactions of **1** with **2**, yielding **3** and its sequential dehydrogenative coupling with **4**, readily afforded **FBTzE**-containing monomers **5a–5c** that have lower lowest unoccupied molecular orbital (LUMO) energy level and smaller energy gap than those of 5,6-difluorobenzothiadiazole (**DFBT**). Subsequently, three types of **FBTzE**-containing copolymers **3T**, **4T**, and **2TTT** were synthesized by Migita–Kosugi–Stille coupling of monomers **5b** and **5c** with distannylated thiophene, bithiophene, and thienothiophene, respectively and their physicochemical properties and solar cell performances were evaluated. As a result of cyclic voltammogram, the synthesized **FBTzE**-based polymers have deeper highest occupied molecular orbital (HOMO) and LUMO energy levels, and stronger intermolecular interactions than those of **DFBT**-based polymer **PffBT4T-DT**. Although **3T**/$PC_{61}BM$ blended film formed favorable face-on orientation with short d_π of 3.57 Å, its solar cell showed poor PCE of 2.7% owing to the construction of large phase separation structure with a domain size over 100 nm. In a sharp contrast, **2TTT**/$PC_{61}BM$ formed unsuitable edge-on orientation with short d_π of 3.49 Å, but its film formed optimal nanoscale phase separation, leading to a good performance with PCE of up to 5.2%.

Received 16th November 2018,
Accepted 18th December 2018

DOI: 10.1039/c8tc05764h

rsc.li/materials-c

Introduction

Donor–acceptor (D–A) type semiconducting polymers have been widely utilized for the development of high-performance p-type and n-type semiconductors in organic field-effect transistors (OFETs)[1,2] and organic photovoltaic cells (OPVs).[3,4] Main advantages of D–A polymers are electron delocalization and the construction of quinoidal structures through a mesomeric effect, leading to broad absorption with a small bandgap (E_g) and strong intermolecular interactions owing to their electrostatic interaction between polymer mainchains.[3,4] In addition, the electronic states (highest occupied molecular orbital (HOMO) and lowest unoccupied molecular orbital (LUMO) energy levels) of D–A polymers can easily be controlled by combining the various donor and acceptor units.[3–5] To date, many researchers have developed the high-performance D–A polymers and achieved high field-effect mobility (μ) over 1 $cm^2\ V^{-1}\ s^{-1}$[6–11] and high power conversion efficiency (PCE) over 10%.[12–17]

In order to obtain the high-performance low-bandgap p-type polymers and air-stable n-type polymers for OFETs and OPVs, the development of strong acceptor units is highly desirable. Among the developed strong acceptors including diketopyrrolopyrrole (DPP),[7,18–20] isoindigo (IID),[21–24] naphthalenediimide (NDI),[25–27] naphthobisthiadiazole (NTz),[13,28] and a double B←N bridged bipyridyl (BNBP),[29–31] 5,6-difluorobenzo[*c*][1,2,5]-thiadiazole (**DFBT**, Fig. 1) is the well-known strong acceptor unit for both high-performance OFETs and OPVs,[15,32–40] because of the following reasons. First, not only the electron-deficient 1,2,5-thidiazole ring and *o*-benzoquinoidal structure of a **DFBT** core, but also two fluorine atoms can offer the low-lying LUMO and HOMO energy level and narrow bandgap.[15,32–40] Therefore, **DFBT**-containing polymers have high air-stability and high light-harvesting ability. Second, since a **DFBT** core can facilitate the intra- and intermolecular non-covalent interactions such as N···H, F···S, and F···H between neighboring aromatic π-spacer or polymer backbones, **DFBT**-based copolymers have high coplanarity with dihedral angles of nearly 0° and can promote the π-orbital overlap between polymer backbones, which can

[a] *Graduate School of Natural Science and Technology, Okayama University, 3-1-1 Tsushimanaka, Kita-ku, Okayama 700-8530, Japan*
[b] *Research Institute for Interdisciplinary Science, Okayama University, 3-1-1 Tsushimanaka, Kita-ku, Okayama 700-8530, Japan. E-mail: ynishiha@okayama-u.ac.jp*

† Electronic supplementary information (ESI) available: Full characterizations, and ^1H, $^{13}C\{^1H\}$, and $^{19}F\{^1H\}$ NMR spectra of all new compounds and polymers, details of theoretical calculations, GPC traces, physicochemical properties, SCLC hole mobility, photovoltaic properties, GIWAXS analysis. See DOI: 10.1039/c8tc05764h

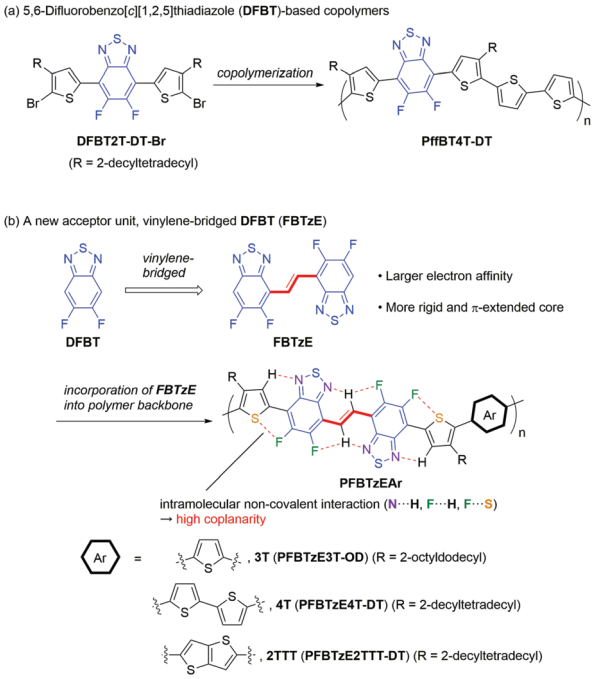

Fig. 1 Chemical structures of **DFBT**, **FBTzE**, and its copolymers.

provide a strong aggregation.[35,41,42] Indeed, it is reported that simple **DFBT**-quaterthiophene copolymers (**PffBT4T-R**, Fig. 1a) exhibited strong temperature-dependent aggregation.[15,33,34,43] Moreover, this strong aggregation behavior can facilitate the high crystalline thin films, resulting in a high field-effect hole mobility of nearly 2 $cm^2\ V^{-1}\ s^{-1}$.[33] In addition, since **DFBT** copolymers also formed the long-range ordered structure even in the blended films with soluble fullerene, space-charge limited current (SCLC) hole mobility reached $10^{-2}\ cm^2\ V^{-1}\ s^{-1}$, and thus the fabricated OPV exhibited excellent PCE of 12%.[15,43]

However, to the best our knowledge, despite these excellent features, new type of **DFBT**-containing acceptor units have not been developed. Therefore, the development of a new class of acceptor unit bearing a **DFBT** unit is highly important to develop the novel high-performance semiconducting polymers for OFETs and OPVs.

In terms of the new high-performance p-type and n-type semiconductors based on a **DFBT** unit, we newly designed and synthesized vinylene-bridged **DFBT** unit (**FBTzE**, Fig. 1b). The presence of two **DFBT** units in the **FBTzE** core might enhance the electron affinity, which can lower HOMO and LUMO energy levels. In fact, the DFT calculation revealed that model compound of **FBTzE**–quaterthiophene copolymer has lower HOMO and LUMO energy levels than those of a **DFBT** counterpart (Fig. S1, ESI†). This feature is highly advantageous for high-performance OPVs and n-type semiconductors. In addition, more rigid and π-extended structure of the **FBTzE** core owing to various intramolecular non-covalent interaction can enhance the effective π-orbital overlaps, compared to those of **DFBT**-based polymers, which may lead to the construction of high crystalline thin-film with longer-range ordered structure.[28] Herein, we report the synthesis of three bis(4-alkylthienyl)**FBTzE** monomers and the three copolymers containing thiophene, bithiophene, and thienothiophene as the spacers (Fig. 1b). In addition, their physicochemical properties, thin-film structure analyses, and solar cell characteristics were investigated to evaluate the potential of **FBTzE** for high-performance semiconducting polymers. Here, each **FBTzE** and bis(4-methylthienyl)**FBTzE** has four possible conformations. From DFT calculations, conformers 1 and 5 is the most thermodynamically stable structure (Fig. S2, ESI†). Thus, we hereafter describe chemical structures of **FBTzE**-based copolymers with these conformations.

Experimental

General

All the reactions were carried out under an Ar atmosphere using standard Schlenk techniques. Glassware was dried in an oven (130 °C) and heated under reduced pressure prior to use. Dehydrated tetrahydrofuran (THF), dimethylsulfoxide (DMSO), and toluene were purchased from Kanto Chemicals Co., Ltd. For thin layer chromatography (TLC) analyses throughout this work, Merck precoated TLC plates (silica gel 60 GF_{254}, 0.25 mm) were used. Silica gel column chromatography was carried out using Silica gel 60 N (spherical, neutral, 40–100 μm) from Kanto Chemicals Co., Ltd. The ^1H, $^{13}C\{^1H\}$, $^{19}F\{^1H\}$ NMR spectra were recorded on a Varian 400-MR (400 MHz) and Varian INOVA-600 (600 MHz) spectrometer. Infrared spectra were recorded on a Shimadzu IRPrestige-21 spectrophotometer. Elemental analyses were carried out with a Perkin-Elmer 2400 CHN elemental analyzer at Okayama University. Polymerizations were performed with a Biotage initiator microwave reactor. Molecular weights of polymers were determined by gel-permeation chromatography (GPC) with a TOSOH HLC-8321GPC/HT and TSKgel GMH_{HR}-H HT using a polystyrene standard and *o*-dichlorobenzene (*o*-DCB) as the eluent at 140 °C. Recycling preparative high performance liquid chromatography (HPLC) was performed on a Shimadzu LC-20AP instrument equipped with Shodex GPC K-4001L and -4002L columns, and Shimadzu RID-10 refractive index detector. Chloroform was used as the mobile phase at room temperature with a flow rate 14 mL min^{-1}.

4-Bromo-5,6-difluorobenzo[*c*][1,2,5]thiadiazole (**1**),[44] 2-bromo-3-(2-hexyldecyl)thiophene (**4a**),[45] 2-bromo-3-(2-octyldodecyl)-thiophene (**4b**),[45] 2-bromo-3-(2-decyltetradecyl)thiophene (**4c**),[46] 2,5-bis(trimethylstannyl)thiophene (**6**),[47] 5,5′-bis(trimethylstannyl)-2,2′-bithiophene (**7**),[48] 2,5-bis(trimethylstannyl)thieno[3,2-*b*]-thiophene (**8**),[49] 5,6-difluorobenzo[*c*][1,2,5]thiadiazole (**DFBT**),[38] 5,6-difluoro-4,7-bis(5-bromo-4-(2-decyltetradecyl)thiophen-2-yl)-benzo[*c*][1,2,5]thiadiazole (**DFBT2T-DT-Br**),[38] and **PffBT4T-DT**[43] were synthesized according to the reported procedures. All other chemicals were used without further purification unless otherwise indicated.

(*E*)-1,2-Bis(5,6-difluorobenzo[*c*][1,2,5]thiadiazol-4-yl)ethene (FBTzE) (3). To a deaerated solution of 4-bromo-5,6-difluorobenzo[*c*][1,2,5]thiadiazole (**1**, 1.18 g, 4.7 mmol) and *trans*-1,2-bis(tributylstannyl)ethylene (**2**, 1.30 g, 2.1 mmol) in anhydrous toluene (105 mL) in a 200 mL two-necked round-bottomed

flask were added tris(dibenzylideneacetone)dipalladium(0)-chloroform adduct ($Pd_2(dba)_3{\cdot}CHCl_3$, 110 mg, 0.11 mmol) and tri(*o*-tolyl)phosphine ($P(o\text{-tolyl})_3$, 130 mg, 0.43 mmol). The reaction mixture was heated to a gentle reflux for 12 h. The resulting mixture was cooled to room temperature and 1 M potassium fluoride (KF) aqueous solution (100 mL) was added. The crude mixture was extracted with chloroform (100 mL × 5) and washed with brine and dried over $MgSO_4$. After the removal of the solvent under reduced pressure, obtained solid was washed with hexane and purified by passing through a pad of Florisil with chloroform as the eluent to afford **3** (772 mg, 2.1 mmol), quantitatively, as a yellow solid. Mp 255–256 °C. FT-IR (KBr, cm^{-1}): 3107 (w), 3074 (w), 1528 (m), 1466 (s), 1350 (m), 1308 (s), 1182 (s), 974 (s), 937 (m), 872 (s), 843 (s), 438 (m). ^1H NMR (600 MHz, $CDCl_3$, rt): δ 7.71 (dd, J = 8.8, 7.2 Hz, 2H), 8.88 (s, 2H). $^{13}C\{^1H\}$ NMR (151 MHz, $CDCl_3$, rt): δ 105.49 (d, J = 19.8 Hz), 116.74 (d, J = 11.5 Hz), 125.46 (dd, J = 6.9, 3.5 Hz), 149.81 (d, J = 8.1 Hz), 150.99 (d, J = 12.7 Hz), 151.45 (dd, J = 262.4, 18.4 Hz), 154.10 (dd, J = 257.9, 18.5 Hz). $^{19}F\{^1H\}$ NMR (376 MHz, $CDCl_3$, rt): δ −131.27 (d, J = 17.3 Hz), −128.28 (d, J = 17.3 Hz). Anal. calcd for $C_{14}H_4F_4N_4S_2$: C, 45.65; H, 1.09; N, 15.21%. Found: C, 45.70; H, 0.88; N, 15.20%.

Typical procedure for the synthesis of (*E*)-1,2-bis(7-(5-bromo-4-(2-hexyldodecyl)thiophen-2-yl)-5,6-difluorobenzo[*c*][1,2,5]-thiadiazol-4-yl)ethene (5a). In a 50 mL Schlenk tube, 2-bromo-3-(2-hexyldecyl)thiophene (**4a**, 1.79 g, 4.6 mmol) was added to a mixture of compound **3** (423 mg, 1.15 mmol), palladium(II) trifluoroacetate ($Pd(tfa)_2$, 77 mg, 0.23 mmol), and silver(I) carbonate (Ag_2CO_3, 2.54 g, 9.2 mmol) in DMSO (11.5 mL). The reaction mixture was stirred at 140 °C for 24 h. After cooling to room temperature, the mixture was extracted with dichloromethane (50 mL × 3), washed with 1 M HCl aqueous solution and brine, and then dried over $MgSO_4$. After the removal of the solvent under reduced pressure, obtained solid was purified by silica gel column chromatography with hexane and hexane–dichloromethane (5 : 1) as the eluents (R_f = 0.41) to afford **5a** (663 mg, 0.58 mmol) in 52% yield as a red solid. Mp 88–90 °C. FT-IR (KBr, cm^{-1}): 2924 (s), 2853 (s), 1541 (m), 1489 (m), 1445 (s), 1354 (m), 982 (m), 851 (m), 536 (m). ^1H NMR (600 MHz, $CDCl_3$, rt): δ 0.89 (t, J = 7.2 Hz, 12H), 1.20–1.40 (m, 48H), 1.67 (m, 2H), 2.42 (d, J = 7.2 Hz, 4H), 7.70 (s, 2H), 8.10 (s, 2H). $^{13}C\{^1H\}$ NMR (150 MHz, $CDCl_3$, rt): δ 14.30, 14.31, 22.87, 22.90, 26.67, 26.70, 29.57, 29.86, 29.93, 30.26, 32.11, 32.12, 33.47, 33.48, 34.09, 38.67, 112.15 (d, J = 11.5 Hz), 113.83 (d, J = 10.4 Hz), 116.06 (d, J = 9.2 Hz), 123.40 (br), 131.24, 132.44 (d, J = 11.6 Hz), 141.75, 148.55 (d, J = 9.2 Hz), 148.99 (d, J = 8.1 Hz), 149.18 (dd, J = 260.1, 19.6 Hz), 151.58 (dd, J = 262.4, 18.4 Hz). $^{19}F\{^1H\}$ NMR (376 MHz, $CDCl_3$, rt): δ −130.98 (d, J = 14.7 Hz), −129.22 (d, J = 14.7 Hz). Anal. calcd for $C_{54}H_{70}Br_2F_4N_4S_4$: C, 56.93; H, 6.19; N, 4.92%. Found: C, 56.98; H, 6.15; N, 4.87%.

(*E*)-1,2-Bis(7-(5-bromo-4-(2-octyldodecyl)thiophen-2-yl)-5,6-difluorobenzo[*c*][1,2,5]-thiadiazol-4-yl)ethene (5b). Red solid. Yield: 45% (hexane : dichloromethane = 5 : 1 as the eluents, R_f = 0.70). Mp 73–75 °C. FT-IR (KBr, cm^{-1}): 2924 (s), 2853 (s), 1543 (m), 1489 (m), 1443 (s), 1354 (m), 984 (m), 851 (m), 536 (m). ^1H NMR (600 MHz, $CDCl_3$, rt): δ 0.87 (t, J = 6.9 Hz, 12H), 1.20–1.40 (m, 64H), 1.71 (m, 2H), 2.50 (d, J = 7.2 Hz, 4H), 7.82 (s, 2H), 8.43 (s, 2H). $^{13}C\{^1H\}$ NMR (100 MHz, $CDCl_3$, rt): δ 14.15, 14.33, 14.49, 22.74, 22.92, 23.08, 26.65, 29.62, 29.64, 29.92, 29.99, 30.34, 31.98, 32.15, 32.32, 33.35, 33.82, 38.60, 111.56 (d, J = 11.5 Hz), 112.98 (d, J = 10.7 Hz), 116.17 (d, J = 9.2 Hz), 122.02 (br), 131.01, 131.79 (d, J = 10.7 Hz), 141.33, 148.02 (d, J = 9.3 Hz), 148.34 (d, J = 8.3 Hz), 148.62 (dd, J = 235.0, 19.1 Hz), 151.22 (dd, J = 235.8, 18.3 Hz). $^{19}F\{^1H\}$ NMR (376 MHz, $CDCl_3$, rt): δ −130.98 (d, J = 14.7 Hz), −129.29 (d, J = 14.7 Hz). Anal. calcd for $C_{62}H_{86}Br_2F_4N_4S_4$: C, 59.51; H, 6.93; N, 4.48%. Found: C, 59.51; H, 6.96; N, 4.39%.

(*E*)-1,2-Bis(7-(5-bromo-4-(2-decyltetradecyl)thiophen-2-yl)-5,6-difluorobenzo[*c*][1,2,5]-thiadiazol-4-yl)ethene (5c). Red solid. Yield: 45% (hexane : dichloromethane = 5 : 1 as the eluents, R_f = 0.80). Mp 62–64 °C. FT-IR (KBr, cm^{-1}): 2924 (s), 2851 (s), 1543 (m), 1489 (m), 1443 (s), 1354 (m), 1342 (m), 1005 (m), 982 (m), 851 (m), 721 (m), 536 (m). ^1H NMR (300 MHz, $CDCl_3$, rt): δ 0.87 (t, J = 6.8 Hz, 12H), 1.20–1.40 (m, 80H), 1.73 (s, 2H), 2.54 (d, J = 7.2 Hz, 4H), 7.89 (s, 2H), 8.61 (s, 2H). $^{13}C\{^1H\}$ NMR (100 MHz, $CDCl_3$, rt): δ 14.32, 14.48, 19.80, 20.99, 22.74, 22.91, 23.08, 26.67, 29.62, 29.63, 29.92, 29.24, 29.98, 30.01, 30.36, 31.99, 32.16, 32.17, 32.33, 33.37, 33.85, 38.61, 43.29, 111.62 (d, J = 10.7 Hz), 113.08 (d, J = 10.7 Hz), 116.17 (d, J = 9.2 Hz), 122.16 (br), 131.04, 131.86 (d, J = 10.8 Hz), 141.38, 148.08 (d, J = 9.2 Hz), 148.42 (d, J = 8.4 Hz), 148.68 (dd, J = 240.5, 19.1 Hz), 151.28 (dd, J = 237.2, 18.3 Hz). $^{19}F\{^1H\}$ NMR (376 MHz, $CDCl_3$, rt): δ −130.97 (d, J = 14.7 Hz), −129.27 (d, J = 14.7 Hz). Anal. calcd for $C_{70}H_{102}Br_2F_4N_4S_4$: C, 61.66; H, 7.54; N, 4.11%. Found: C, 61.67; H, 7.76; N, 4.09%.

Typical procedure for the synthesis of polymers (PFBTzE3T-OD, 3T). Monomers **5b** (62.6 mg, 0.05 mmol), 2,5-bis(trimethylstannyl)thiophene (**6**, 20.5 mg, 0.05 mmol), tetrakis(triphenylphosphine)palladium(0) ($Pd(PPh_3)_4$, 1.2 mg, 1 μmol), copper iodide(I) (CuI, 1.0 mg, 5 μmol) and toluene (2.5 mL) were added to a reaction vessel, which was sealed and refilled with argon. The reaction mixture was heated at 180 °C for 2 h in a microwave reactor. After being cooled to room temperature, the reaction mixture was poured into 100 mL of methanol containing 5 mL of concentrated hydrochloric acid and stirred for 3 h. The precipitate was then subjected to sequential Soxhlet extraction with methanol, hexane, and chloroform to remove low molecular-weight fractions. The residue was extracted with chlorobenzene, and concentrated solution was poured into 50 mL of methanol. The formed precipitates were collected by filtration and dried *in vacuo* to afford **3T** (44.7 mg, 76%) as a metallic purple solid. GPC (*o*-DCB, 140 °C): M_n = 46.9 kDa, M_w = 93.1 kDa, PDI = 1.98. Anal. calcd for $C_{66}H_{90}F_4N_4S_5$: C, 67.42; H, 7.72; N, 4.77%. Found: C, 66.86; H, 7.52; N, 4.61%.

PFBTzE4T-DT, 4T. Monomers **5c** (68.2 mg, 0.05 mmol), 5,5′-bis(trimethylstannyl)-2,2′-bithiophene (**7**, 24.6 mg, 0.05 mmol), tetrakis(triphenylphosphine)palladium(0) (1.2 mg, 1 μmol), and toluene (2.5 mL) were subjected to the polymerization procedure, and the reaction mixture was heated at 140 °C for 30 min in a microwave reactor. Sequential Soxhlet extraction with the same solvents used for **3T** was employed to obtain **4T** (40.6 mg, 59%) as

a metallic purple solid. GPC (*o*-DCB, 140 °C): M_n = 133.8 kDa, M_w = 319.8 kDa, PDI = 2.39. Anal. calcd for $C_{78}H_{108}F_4N_4S_6$: C, 68.38; H, 7.95; N, 4.09%. Found: C, 68.37; H, 8.01; N, 3.94%.

PFBTzE2TTT-DT, 2TTT. Monomers **5c** (68.2 mg, 0.05 mmol), 2,5-bis(trimethylstannyl)thieno[3,2-*b*]thiophene (**8**, 23.3 mg, 0.05 mmol), tetrakis(triphenylphosphine)palladium(0) (1.2 mg, 1 μmol), and toluene (2.5 mL) were subjected to the polymerization procedure, and the reaction mixture was heated at 140 °C for 30 min in a microwave reactor. Sequential Soxhlet extraction with the same solvents used for **3T** was employed to obtain **2TTT** (39.9 mg, 59%) as a metallic purple solid. GPC (*o*-DCB, 140 °C): M_n = 76.4 kDa, M_w = 166.7 kDa, PDI = 2.18. Anal. calcd for $C_{76}H_{106}F_4N_4S_6$: C, 67.91; H, 7.95; N, 4.17%. Found: C, 67.65; H, 7.95; N, 3.92%.

Instrumentation and theoretical calculation

UV-vis absorption spectra were measured using a Shimadzu UV-2450 UV-vis spectrometer. Cyclic voltammograms (CVs) were recorded on Electrochemical Analyzer CHI-600B in acetonitrile containing tetrabutylammonium hexafluorophosphate (TBAP, 0.1 M) as supporting electrolyte at a scan rate of 100 mV s^{-1}. A Pt electrode (surface area: A = 0.071 cm^2, BAS), an Ag/Ag^+ (Ag wire in 0.01 M $AgNO_3$/0.1 M $TBAPF_6/CH_2Cl_2$ or CH_3CN), and a Pt wire electrode were used as working, reference, and counter electrodes, respectively. Samples of the polymer films were prepared by drop-casting on a working electrode from their chloroform solutions. All the potentials were calibrated with the standard ferrocene/ferrocenium redox couple (Fc/Fc^+: $E^{1/2}$ = +0.52 V for CH_2Cl_2, and $E^{1/2}$ = +0.01 V for CH_3CN measured under identical conditions). Dynamic force-mode atomic force microscopy was carried out using an SPA 400-DFM (SII Nano Technologies). Grazing incidence wide-angle X-ray diffraction (GIWAXS) analyses were carried out at SPring-8 on beamline BL46XU. The samples were irradiated at a fixed angle on the order of 0.12° through a Huber diffractometer with an X-ray energy of 12.39 keV (λ = 1 Å), and the GIWAXS patterns were recorded on a 2D image detector (Pilatus 300K). Films of the polymers and blended films with $PC_{61}BM$ were fabricated by spin-coating on the ZnO treated ITO substrate. Geometry optimizations and normal-mode calculations were performed at the B3LYP/6-31G(d) or M06-2X/6-31G** level using the Gaussian 09, Revision D.01, program package.[50]

Fabrication of inverted bulk-heterojunction solar cells

The inverted bulk-heterojunction solar cells were fabricated as follows. ZnO precursor solution was prepared by hydrolysis of $Zn(OAc)_2$.[51] The ITO substrates (ITO, Geomatec Co. Ltd, thickness = 150 nm, sheet resistance $< 12\ \Omega\ sq^{-1}$, transmittance (λ = 550 nm) $\geq$ 85%) were successively washed using ultrasonication in a neutral detergent, deionized water, acetone, and isopropanol at room temperature, and in hot isopropanol, for 10 min, respectively. Then ITO substrates were treated with UV-ozone for 20 min. Pre-cleaned ITO substrates were spin-coated with 0.4 M ZnO precursor solution at 4000 rpm for 30 s, and then immediately baked at 200 °C for 30 min in air. After gradual cooling to room temperature, the substrates were rinsed with acetone and isopropanol at room temperature, then in hot isopropanol for 5 min. The substrates were dried and immediately transferred into a nitrogen-filled glove box. The active layers with $PC_{61}BM$ were deposited by spin-coating (at 600 rpm for 60 s for **3T**, and at 600 rpm for 30 s for **4T** and **2TTT**) from a solution containing a polymer sample (10.0 mg mL^{-1} for **3T**, 3.3 mg mL^{-1} for **4T**, and 6.0 mg mL^{-1} for **2TTT**) and a respective amount of $PC_{61}BM$ in anhydrous chlorobenzene (CB). The solution was kept at 100–140 °C (100 °C for **3T**, and 140 °C for **4T** and **2TTT**) for 30 min, and the hot solution was spin-coated on the substrate (at room temperature for **3T**, and preheated at 140 °C for **4T** and **2TTT** before spin-coating). The p/n ratio denotes weight ratios of polymers and $PC_{61}BM$. 1,8-Diiodooctane (DIO, 1 vol% for **4T**) or diphenyl ether (DPE, 2.5 vol% for **3T** and 4 vol% for **2TTT**) were used as the solvent additives. The active layer thickness of **3T** and **2TTT** was 100 and 130 nm, respectively. The uniform **4T**/$PC_{61}BM$ blended film could not be obtained, due to too strong aggregation tendency of **4T**. MoO_3 (6 nm) as an anode interlayer and an Ag (50 nm) layer were deposited under high vacuum ($\sim 6 \times 10^{-5}$ Pa) through a shadow mask. The active area of all devices was 0.16 cm^2. The thickness of the active layer was measured with an AlphaStep® IQ surface profiler (KLA Tencor).

The characteristics of the solar cell devices were measured through a 4 × 4 mm photo-mask, with a Keithley 2401 semiconductor analyzer, using a Xe lamp (Bunkokeiki OTENTO-SAN III type G2) as the light source, under AM 1.5 G simulated solar irradiation at 100 mW cm^{-2} at room temperature under a nitrogen atmosphere. The light intensity was determined by a calibrated standard silicon solar cell (Bunkokeiki, BS-520BK). External quantum efficiency (EQE) was measured using a Bunkokeiki SM-250 Hyper Monolight System.

Fabrication and characterization of hole-only devices

Hole-only devices were fabricated as follows. ITO substrates were washed and treated with UV-ozone in the same manner as described above. Then, ITO substrates were spin-coated with poly(3,4-ethylene-dioxythiophene):poly(styrene sulfonate) (PEDOT:PSS) (Clevios P VP AI 4083) through a 0.45 μm PVDF syringe filter at 5000 rpm for 30 s, and dried at 120 °C for 10 min in air. After being dried, the substrates were immediately transferred into a nitrogen-filled glove box. Thin films of an active layer were deposited by same procedure as described above (high concentration solution was used, 13.3 mg mL^{-1} for **3T** and 8.0 mg mL^{-1} for **2TTT**). The active layer thickness of **3T** and **2TTT** was 240 and 220 nm, respectively. After the thin films were dried, MoO_3 (6 nm) and Al (80 nm) layers with an active cathode area of 0.16 cm^2 were deposited under high vacuum ($\sim 6 \times 10^{-5}$ Pa) through a shadow mask.

Current density–voltage (J–V) characteristics of the fabricated devices were measured using a Keithley 2401 Source Meter in the dark. Voltage sweeps were performed in the range of 0–8 V, and hole mobilities were estimated from the J–V curve of the Mott–Gurney space charge limited current (SCLC) law:[52]

$$J = (9/8)\varepsilon_0\varepsilon_r\mu(V^2/L^3) \quad (1)$$

where ε_0 is the permittivity of free space, ε_r is the dielectric constant of the polymer, μ is the hole mobility, L is the thickness of the active layer, and V is the voltage drop across the device ($V = V_{appl} - V_{bi}$). ε_r is assumed to be 3, which is a typical value for semiconducting polymers.

Results and discussion

Synthesis of FBTzE derivatives and FBTzE-based copolymers PFBTzEAr

Scheme 1 shows synthetic routes of **FBTzE 3**, monomers **5a–5c**, and three copolymers. Migita–Kosugi–Stille coupling of 4-bromo-5,6-difluorobenzo[*c*][1,2,5]thiadiazole (**1**)[44] and *trans*-1,2-bis(tributylstannyl)ethylene (**2**) afforded **FBTzE** (**3**) quantitatively. Then, **FBTzE**-containing monomers **5a–5c** were synthesized by dehydrogenative coupling of **3** with 2-bromo-3-(2-alkyl)thiophenes **4a–4c**.[44,53,54] After optimization of the palladium catalyst, oxidant, and additive, we could obtain compound **5a** in 51% isolated yield (Table S1, ESI†). Accordingly, with the same reaction conditions in hand, monomers **5b** and **5c** with different side chains were also synthesized. When **5a** was used for copolymerization with distannylated bithiophene **7**, soluble polymers were not obtained due to its insufficient solubility. Therefore, Migita–Kosugi–Stille coupling reactions of **5b** with distannylated thiophene **6**, and of **5c** with distannylated bithiophene **7** and thienothiophene **8** yielded three copolymers **PFBTzEAr** in 76% (**Ar** = **3T**), 59% (**Ar** = **4T**), and 59% (**Ar** = **2TTT**), respectively. In the case of **3T**, the addition of CuI and longer time were needed to obtain high-molecular-weight polymer. From high-temperature gel-permeation chromatography (GPC) analyses, all three polymers have high molecular weight over 40 kDa. Among them, the number-average molecular weights (M_n) of **4T** and **2TTT** polymers (M_n = 133.8 and 76.4 kDa) are significantly higher than that of **3T** (M_n = 46.9 kDa). This result might be attributed to the high aggregation in the solution. In fact, GPC curves of **4T** and **2TTT** showed obvious dual peaks at high and low retention time region, and M_n of the polymer obtained from a low-concentration solution of **4T** and **2TTT** become a lower value than that from high-concentration solution (Fig. S5 and Table S2, ESI†). Therefore, polymers **4T** and **2TTT** have stronger intermolecular interaction, likely due to their higher symmetry of polymer backbones.[55]

Computational study of FBTzE and its derivatives

In order to evaluate the non-covalent intermolecular interaction, the optimized structures of several model compounds were calculated by density functional theory (DFT) using M06-2X/6-31G** level.[35] Fig. 2 shows the optimized structures and dihedral angles of non-substituted and fluorinated *trans*-stilbenes, vinylene-bridged benzothiadiazoles, and **FBTzE** derivatives. *trans*-Stilbene (**I**) has a large dihedral angle of 18.2° between benzene rings and a vinylene moiety owing to a steric repulsion of each hydrogen atom (Fig. 2a). On the other hand, by introducing fluorine atoms or a fused thiadiazole ring instead of two hydrogen atoms, the dihedral angles of fluorinated *trans*-stilbene (**II**) and vinylene-bridged benzothiadiazole (**III**) were drastically decreased to 0.67° and 0.05°, respectively (Fig. 2b and c). This suggests that N···H or F···H interaction can increase the coplanarity of a **FBTzE** framework. Especially, N···H can provide the higher coplanarity than that of F···H, likely due to the existence of stronger hydrogen bond. Furthermore, **FBTzE** (**3**) with both thiadiazole ring has a completely coplanar structure with a dihedral angle of 0° (Fig. 2d). In thiophene-containing compounds, bisthienyl-*trans*-stilbene (**IV**) also has a large dihedral angle of 27.2° between benzene and adjacent thiophene rings (Fig. 2e). On the other hand, model compounds **V** and **VI** have largely decreased dihedral angles of 18.8° and 13.9°, respectively, but they do not have completely planar structures (Fig. 2f and g). In contrast, the dihedral angle of bisthienyl **FBTzE** (**VII**) is less than 1°, indicating that both N···H and F···S interactions are required to afford the completely planar structure (Fig. 2h). These N···H and F···S interactions between

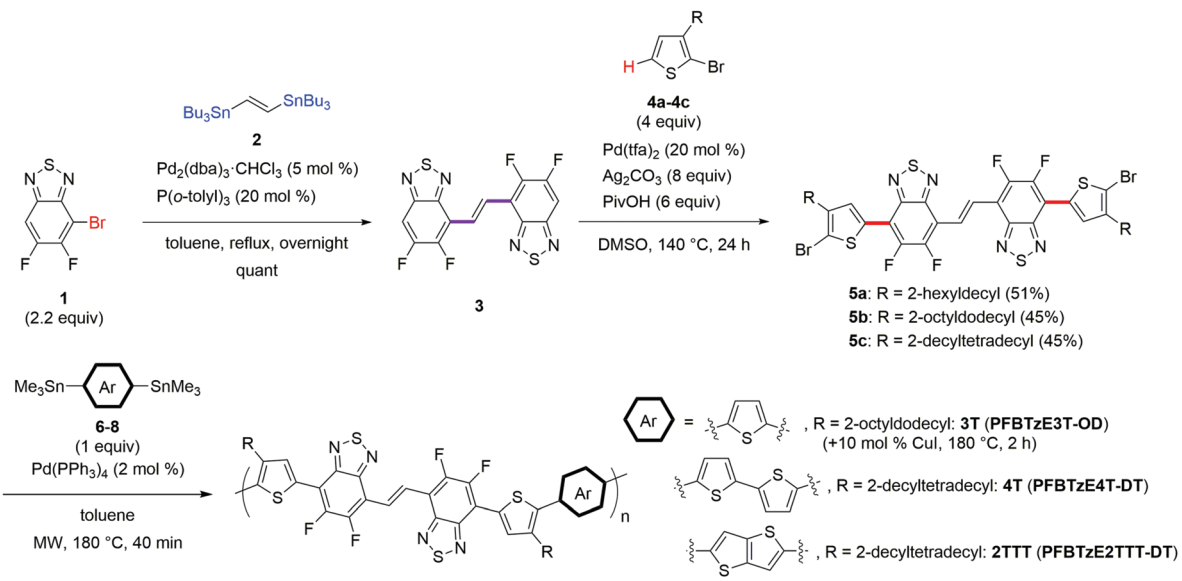

Scheme 1 Synthesis of **FBTzE 3**, monomers **5a–5c**, and copolymers.

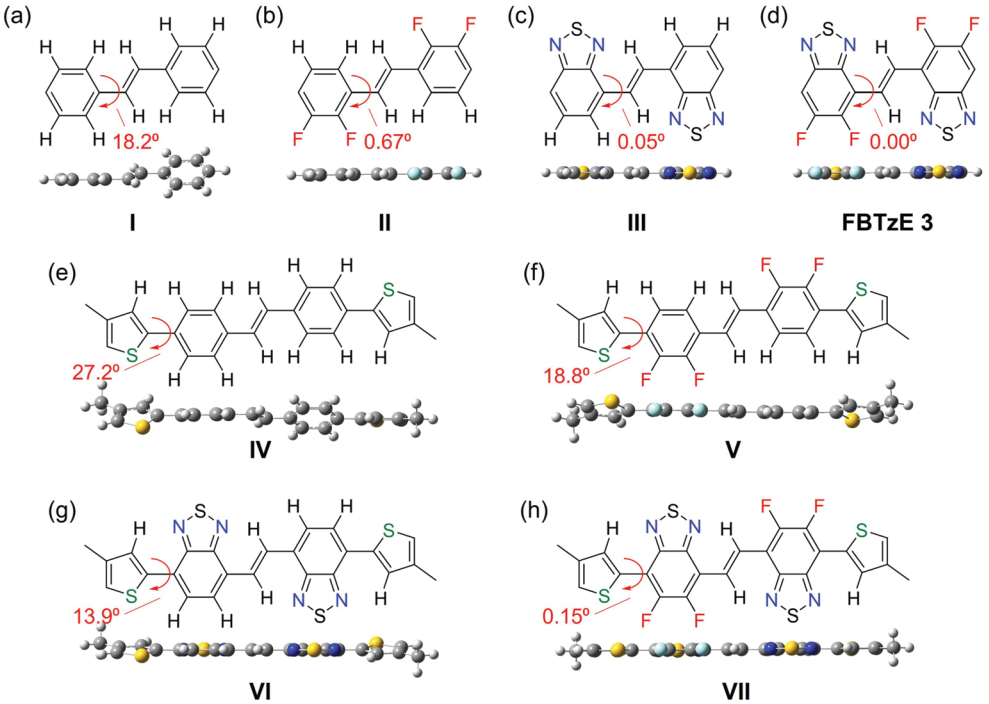

Fig. 2 The optimized molecular structures and calculated dihedral angles of model compounds by DFT using M06-2X/6-31G** level.

benzothiadiazole derivatives and neighboring thiophene ring is well-known and evaluated by single-crystal structure analyses.[42,56,57] These calculation results are consistent with previously reported results. From these results, highly coplanar structure of **FBTzE** and its derivative can be expected to give the densely packing structure in the solid state.

Physicochemical properties of FBTzE derivatives

UV-vis absorption spectra and cyclic voltammograms of **3** and monomers **5b** and **5c** are shown in Fig. 3a and b, respectively, and the results are summarized in Table 1, comparing the physicochemical properties of the standard **DFBT** and **DFBT**-containing monomer (**DFBT2T-DT-Br**, Fig. 1a) (Fig. S6a and b, ESI†). The UV-vis absorption spectrum of **3** showed the absorption maximum at 385 nm, which is 78 nm red-shifted absorption than that of **DFBT**. In addition, the optical energy gap (E_g) of **3** (2.80 eV) is significantly smaller than that of **DFBT** (3.71 eV), indicating the effective π-extension of a **FBTzE** core. In monomers **5b** and **5c**, the 31 nm red-shifted absorption (483 nm) and about 0.2 eV smaller E_g were observed, compared to those of **DFBT2T-DT-Br**. Furthermore, the absorption coefficients of **5b** and **5c** are *ca.* 3.5 times higher ($\sim$55 000 M^{-1} cm^{-1}) than that of **DFBT2T-DT-Br**. This results indicates that **FBTzE** derivatives **5b** and **5c** have stronger absorption, which is beneficial for solar cells.

The electrochemical properties of **3** and monomers **5b** and **5c** were investigated (Fig. 3b and Table 1). **FBTzE** (**3**) exhibited clear one oxidation and reduction waves. The estimated HOMO and LUMO energy levels are −6.20 and −3.26 eV, respectively, both of which are lower than those of **DFBT** (HOMO = −6.03 eV and LUMO = −2.98 eV). This indicates that **3** has a larger electron affinity due to the existence of two **DFBT** moieties in its core.

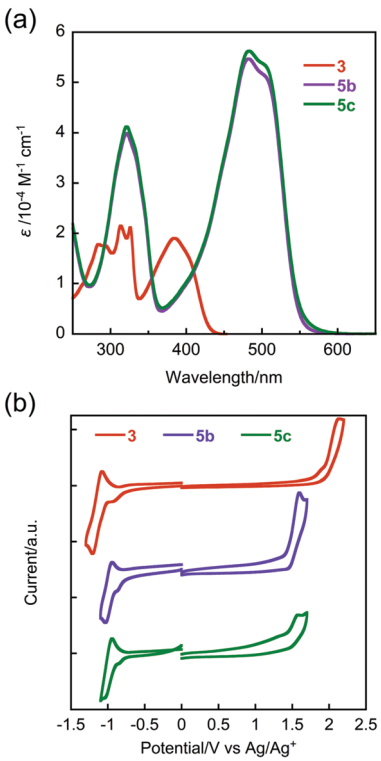

Fig. 3 (a) UV-vis absorption spectra and (b) cyclic voltammograms of **3** and monomers **5b** and **5c** in CH_2Cl_2 solution.

On the other hand, **5b** and **5c** have significantly higher HOMO energy levels around −5.7 eV, and their LUMO energy level are slightly lower than that of **3**. From DFT calculations, the

Table 1 Physicochemical properties of **FBTzE** and **DFBT** derivatives

Compound	$\lambda_{max,sol}$[a]/nm	$\lambda_{max,film}$[b]/nm	E_g^{opt} (E_g^{CV})[c]/eV	E_{HOMO}[d]/eV	E_{LUMO}[e]/eV
3	385	—	2.80 (2.94)	−6.20	−3.26
5b	483, 506	—	2.16 (2.29)	−5.69	−3.40
5c	483, 506	—	2.13 (2.28)	−5.68	−3.40
3T	629, 693	632, 685	1.56 (1.74)	−5.45	−3.71
4T	643, 704	636, 698	1.55 (1.64)	−5.33	−3.69
2TTT	648, 708	644, 707	1.54 (1.64)	−5.35	−3.71
DFBT	307	—	3.71 (3.05)	−6.03	−2.98
DFBT2T-DT-Br	317, 452	—	2.34 (2.40)	−5.71	−3.31
PffBT4T-DT	599, 695	637, 698	1.58 (1.63)	−5.25	−3.62

[a] Absorption maxima in dichloromethane or chlorobenzene solution at rt. [b] Absorption maxima in thin film. [c] Optical energy gap estimated from absorption edge (λ_{edge}) (out of parentheses) and electrochemical gap (in parentheses). [d] All the potentials were calibrated with the standard ferrocene/ferrocenium redox couple (Fc/Fc$^+$: $E^{1/2}$ = +0.52 V for CH_2Cl_2 (small molecules), and $E^{1/2}$ = +0.01 V for CH_3CN (polymer) measured under identical conditions). Estimated with the oxidation onset *vs.* Ag/Ag$^+$; E_{HOMO} = −4.28 or −4.79 − E_{onset}^{ox}. [e] Estimated with the reduction onset *vs.* Ag/Ag$^+$; E_{LUMO} = −4.28 or −4.79 − E_{onset}^{red}.

coefficient of LUMO in **5b** and **5c** strongly localized on the central **FBTzE** core, but a HOMO coefficient delocalized on the entire the molecules (Fig. S3, ESI†). Therefore, the difference of LUMO energy level between **3** and monomers **5b** and **5c** is rather small.[58] Such tendency is in a good agreement with DFT calculations (Fig. S1, ESI†). Compared to **DFBT2T-DT-Br**, **5b** and **5c** exhibited lower LUMO and similar HOMO energy levels, indicating the π-extension of with two **FBTzE** cores, which is consistent with the result of UV-vis absorption spectra.

Physicochemical properties of FBTzE-based copolymers, 3T, 4T, and 2TTT

UV-vis absorption spectra of **PFBTzEAr** polymers are depicted in Fig. 4a and b, and the extracted parameters are also summarized in Table 1. Fig. S6c (ESI†) also showed absorption spectra of **DFBT**-based polymer **PffBT4T-DT** for the comparison. **4T** has the almost similar E_g (1.55 eV) to that of the representative reported polymer **PffBT4T-DT** (1.58 eV) in the solid state (Fig. 4b and Fig. S6c, ESI†).

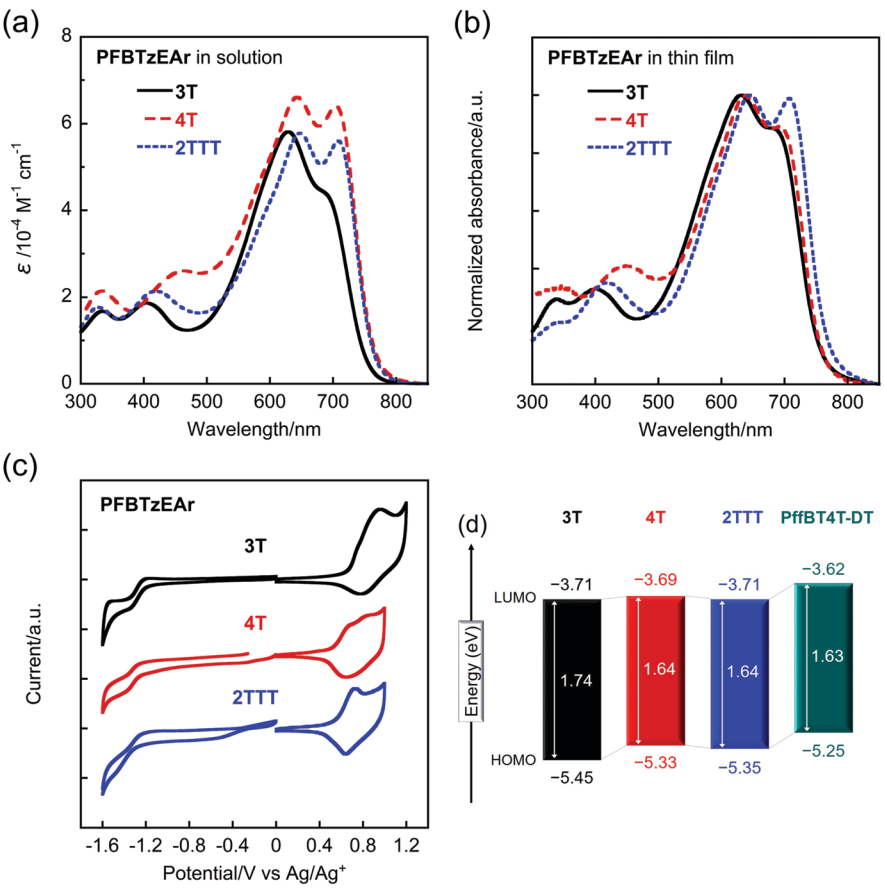

Fig. 4 UV-vis absorption spectra in solution (a) and in thin film (b). (c) Cyclic voltammograms in thin film of polymers **3T**, **4T**, and **2TTT** and (d) their energy diagrams.

One possible reason for such similar E_g may be a similar effective π-conjugation length. In fact, DFT calculations of their model compounds revealed that the difference of E_g between **4T** and **PffBT4T-DT** decreased with an increase of repeating units (Fig. S1, ESI†). Interestingly, both **4T** and **PffBT4T-DT** showed strong temperature-dependent aggregation, but quite different behaviors were observed (Fig. S6c and S7b, ESI†). Upon heating at *ca.* 80 °C in solution, **4T** exhibited a slight blue-shifted spectra and the decrease of an intensity, while **PffBT4T-DT** showed significantly hypochromic shifted absorption spectrum and one broad absorption at longer wavelength region, indicating that **4T** formed partial aggregate in the high temperature solution, whereas **PffBT4T-DT** showed completely disaggregated behavior. These results suggest that **4T** has stronger intermolecular interaction than that of **PffBT4T-DT** due to its extended π-electron system. Cyclic voltammograms of polymers revealed that **4T** have lower HOMO and LUMO energy levels (−5.33 and −3.69 eV) than those of **PffBT4T-DT** (−5.25 and −3.62 eV) (Table 1, Fig. 4c, d and Fig. S6d, ESI†). This may be attributed to a larger electron affinity of the **FBTzE** core, which are consistent with DFT calculations. Such low-lying HOMO and LUMO energy levels of **FBTzE**-based polymers are beneficial for the development of high-performance p-type polymers and n-type semiconductors in OPVs.

All the three polymers **3T**, **4T**, and **2TTT** exhibited similar absorption spectra with almost same E_g (Fig. 4a, b and Table 1). The intensity in absorption spectra of **4T** and **2TTT** was significantly decreased (Fig. S7 and Table S3, ESI†). This indicates that polymers **4T** and **2TTT** have partial aggregation in the high-temperature solution, and thus have a strong intermolecular interaction. In thin film, the absorption spectrum of **2TTT** is identical to that of its room-temperature solution, indicating that **2TTT** formed the highly ordered packing structure in room-temperature solution. On the other hand, the absorption spectrum of **4T**-based film showed slightly blue-shifted compare to room-temperature solution. One possible reason for such difference may be attributed to the different packing motif in the solid state. Such tendency is also observed in high molecular-weight **PffBT4T-DT**,[33] but actual reason has not been described. Polymer **3T** has a similar absorption before and after heating. In addition, the spectrum of **3T** in solution at room temperature is almost identical to that in its thin film. This suggests that **3T** seems to form large aggregate even in the high-temperature solution, which is inconsistent with the result of GPC trace. Polymer **3T** has a higher solubility and lower viscosity in high concentration solution than that of the other polymers **4T** and **2TTT**. In addition, **3T** showed 10–20 nm blue-shifted spectra than that of **4T** and **2TTT**. From these results, we concluded that **3T** did not form large aggregate in the room-temperature solution and has weaker intermolecular interactions. One possible reason for such difference among three polymers is their symmetry of the polymer backbones. From DFT calculations of a dimer structure, **3T** formed a twisted backbone due to the steric hindrance between two alkyl side chains onto terthiophene unit, whereas **4T** and **2TTT** have a relatively coplanar structure owing to their higher regioregularity (Fig. S4, ESI†). Such coplanar structure can enhance the effective π–π overlaps, resulting in a stronger aggregation ability. On the other hand, polymer **3T** has 0.1 eV deeper HOMO and same LUMO energy levels as those of polymers **4T** and **2TTT** (Fig. 4c, d and Table 1). This may be attributed to its twisted backbone to diminish the effective π–π overlap[59,60] or arising from the terthiophene unit having the reduced electron-donating ability.[61]

Photovoltaic properties of polymer/$PC_{61}BM$-based solar cells

To evaluate the potential of **FBTzE** for high-performance electronics, typical inverted solar cells with device structure of ITO/ZnO/(polymer:$PC_{61}BM$)/MoO_3 (6 nm)/Ag (50 nm) were fabricated and characterized. Typical current density (J)–voltage (V) characteristics of the fabricated solar cells under AM 1.5 G simulated solar irradiation at 100 mW cm^{-2} are depicted in Fig. 5a, and the extracted solar cell parameters are summarized in Table 2 and Table S4 (ESI†). The solar cell based on **4T** did not show photovoltaic

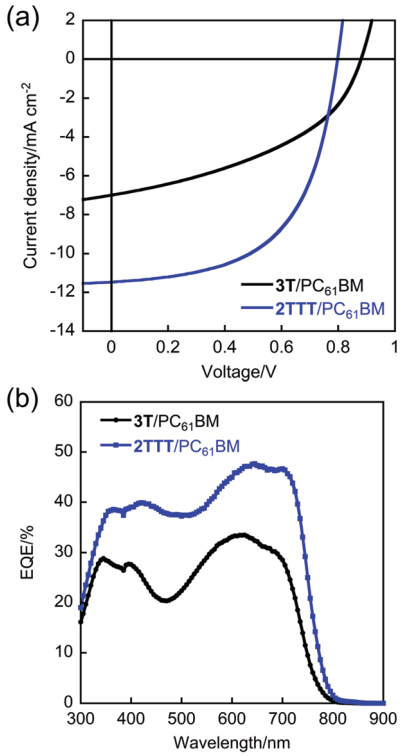

Fig. 5 (a) J–V curves and (b) EQE spectra of **3T** and **2TTT**/$PC_{61}BM$-based solar cells.

Table 2 Solar cell performances of polymer/$PC_{61}BM$-based devices[a]

Device[b]	J_{sc}/mA cm^{-2}	V_{oc}/V	FF	PCE (PCE$_{avg}$)/%
3T	7.00	0.88	0.43	2.66 (2.60)
2TTT	11.47	0.80	0.57	5.23 (5.09)

[a] Average values are shown in parentheses. [b] For **3T**, the polymer/$PC_{61}BM$ blend ratio is 1 : 1 (w/w), solvent = chlorobenzene (CB) + 2.5 vol% diphenyl ether (DPE); for **2TTT**, the polymer/$PC_{61}BM$ blend ratio is 1 : 2 (w/w), solvent = CB + 4 vol% DPE.

response due to the current leakage, because uniform thin-film was not fabricated due to its strong aggregation behavior. The best p/n ratio of **3T** and **2TTT**-based devices were found to be 1 : 1 and 1 : 2. The best solar cell performances were obtained, when the substrate temperatures were room temperature for **3T** and 140 °C for **2TTT**, respectively (Table S5, ESI†). Both **3T**- and **2TTT**-based devices without optimization exhibited poor solar cell performances with PCE of 0.87% for **3T** and 3.09% for **2TTT**, respectively, due to their low short-circuit current density (J_{sc}) and fill factor (FF). When 2.5% and 4% of diphenyl ether (DPE) were used as the solvent additive in **3T** and **2TTT**-based solar cells, respectively, the best OPV performances were observed. Since **3T** has a deeper HOMO energy level, its solar cell exhibited higher open-circuit voltage (V_{oc}) (0.88 V) than that of **2TTT**-based solar cell (0.80 V). However, **2TTT**-based cell showed significantly higher J_{sc} (11.47 mA cm^{-2}) and FF (0.57) than those of **3T**-based cell (J_{sc} = 7.00 mA cm^{-2}, FF = 0.43), and thus higher PCE of 5.23%. From EQE spectra, **2TTT**-based solar cell has a higher photocurrent conversion with maximum EQE of 48% in all regions, compared to the **3T**-based device (Fig. 5b), leading to a high J_{sc}. In order to understand the difference of solar cell performances between **3T** and **2TTT**, the hole-only devices with the device configuration of ITO/(PEDOT:PSS)/(polymer:$PC_{61}BM$)/MoO_3 (6 nm)/Al (80 nm) were fabricated and characterized to estimate their SCLC hole mobility (Fig. S8, ESI†). However, despite higher FF, SCLC hole mobility of the **2TTT**-based hole-only device ($\mu_h = 5.40 \times 10^{-5}$ cm^2 V^{-1} s^{-1}) is lower than that of **3T**-based device ($\mu_h = 7.66 \times 10^{-5}$ cm^2 V^{-1} s^{-1}). We speculated that poor mobility balance of **3T**-based device may lead to low FF, because such mobility balance strongly affects FF of solar cells.[62]

GIWAXS measurement and surface morphology of pure polymer and polymer/$PC_{61}BM$ blended films

In order to evaluate their structure–property relationships, grazing incidence wide-angle X-ray scattering (GIWAXS) and atomic force microscopy (AFM) measurements of polymer/$PC_{61}BM$ blended films were carried out (Fig. 6, 7 and Table S6, ESI†). In pure

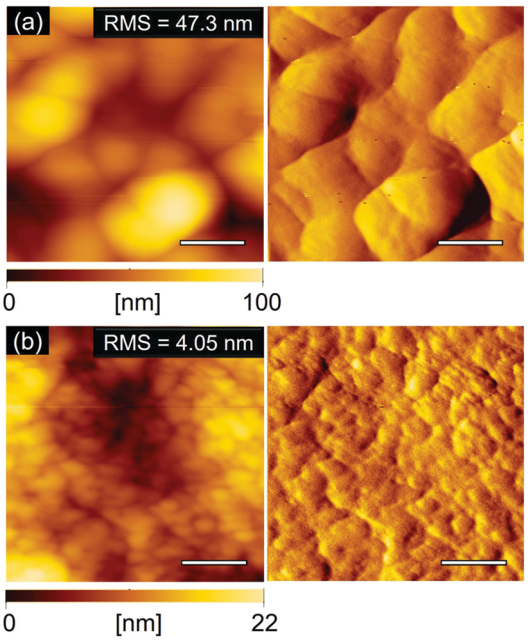

Fig. 7 Topological (left) and error-signal (right) images of polymer/$PC_{61}BM$ blended films on ITO/ZnO substrate; (a) **3T**/$PC_{61}BM$ (p/n = 1 : 1, CB + 2.5 vol% DPE), and (b) **2TTT**/$PC_{61}BM$ (p/n = 1 : 2, CB + 4 vol% DPE). Scale bar is 500 nm.

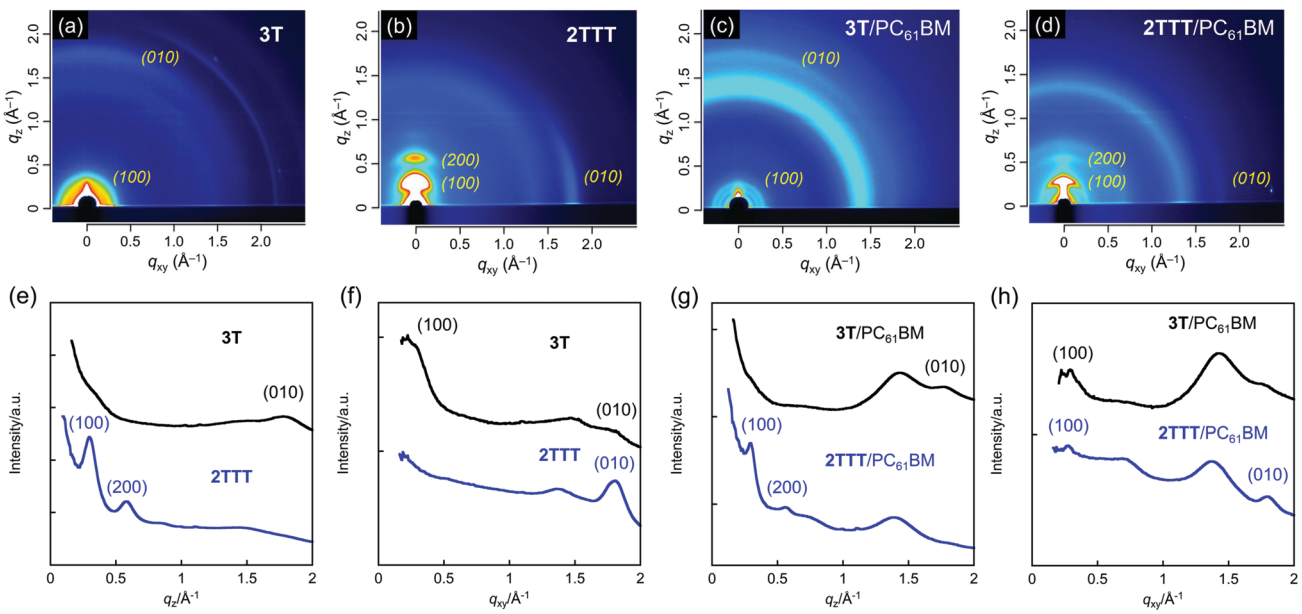

Fig. 6 2D GIWAXS images of (a and b) polymer and (c and d) polymer/$PC_{61}BM$ blended films on ITO/ZnO substrate; (a) **3T**, (b) **2TTT**, (c) **3T**/$PC_{61}BM$ (p/n = 1 : 1, CB + 2.5 vol% DPE), and (d) **2TTT**/$PC_{61}BM$ (p/n = 1 : 2, CB + 4 vol% DPE). 1D cross-sectional profiles of (e and f) pure polymer films and (h and g) polymer/$PC_{61}BM$ blended films on ITO/ZnO substrate; (e and g) out-of-plane and (f and h) in-plane.

polymer films, **3T** film showed weak lamellar diffraction (100) at 0.300 $Å^{-1}$ in q_{xy} axis and π-stacking diffraction (010) at 1.777 $Å^{-1}$ in q_z axis (Fig. 6a, e and f). From these diffractions, **3T** formed a favorable face-on orientation with short π-stacking distance (d_π) of 3.54 Å. In addition, **3T**/$PC_{61}BM$ blended film also formed predominantly face-on orientation with almost same lamellar distance (d_{lm}) of 21.1 Å and short d_π of 3.57 Å (Fig. 6c, g and h). Although **3T** has favorable molecular orientation in both pure polymer and blended film with $PC_{61}BM$, it formed large-scale phase separation with the domain size of 300–500 nm (Fig. 7a). Such unfavorable phase separation structure must prevent the effective photocurrent generation, leading to a poor J_{sc}.[63,64] In contrast, **2TTT** exhibited strong lamellar diffraction (100) at 0.298 $Å^{-1}$ in q_z axis and π-stacking diffraction (010) at 1.805 $Å^{-1}$ in q_{xy} axis, which are completely opposite direction compared to **3T** film (Fig. 6b, e and f). This indicates that **2TTT** formed unsuitable edge-on orientation with a short d_π of 3.48 Å. Moreover, **2TTT**/$PC_{61}BM$ blended film also exhibited almost same diffraction patterns with almost same lamellar distance (d_{lm}) of 21.5 Å and short d_π of 3.49 Å (Fig. 6d, g and h). Such unfavorable orientation may limit the efficient carrier transport, leading to low hole mobility. However, **2TTT**/$PC_{61}BM$ blended film formed well-separated phase separation with a smaller domain size (Fig. 7b). Therefore, **2TTT**-based cell showed higher J_{sc} than that of **3T**-based cell, resulting in a higher PCE.

Conclusions

In summary, we have successfully synthesized **FBTzE** as a new class of acceptor units *via* Migita–Kosugi–Stille coupling and dehydrogenative coupling. In addition, three **FBTzE**-based copolymers, **3T**, **4T**, and **2TTT** were also synthesized. **FBTzE**-containing compounds showed lower LUMO energy levels and smaller E_g than those of a standard **DFBT** core, due to its larger electron affinity and π-extended core. In addition, **FBTzE**-based copolymers have lower-lying HOMO and LUMO energy levels, stronger interaction than those of the parent **DFBT**-based polymer **PffBT4T-DT**, which are beneficial for high-performance electronics. Among the three polymers, **2TTT**-based solar cell exhibited good solar cell performance with PCE of 5.23%, although **2TTT** formed unfavorable edge-on orientation with short d_π of 3.49 Å. Thus, the **FBTzE** core is a potential building block for high-performance D–A semiconducting polymers. Currently, we are investigating to improve the molecular orientation by optimizing solubilizing side chains and donor units.

Conflicts of interest

There are no conflicts to declare.

Acknowledgements

This study was partly supported by ACT-C, JST Grant JPMJCR12YW, Japan, Grant-in-Aid for Scientific Research on Innovative Areas, ''New Polymeric Materials On the basis of Element-Blocks (No. 2401)'', MEXT, Grant 15H00751, Japan, Electric Technology Research Foundation of Chugoku, Chugoku Regional Innovation Research Center, and JKA through its promotion funds from KEIRIN RACE (2018M-184). The GIWAXS experiments were performed at BL46XU of SPring-8 with the approval of the Japan Synchrotron Radiation Research Institute (JASRI) (Proposals 2017A1771 and 2017B1831). We gratefully thank Prof. Itaru Osaka and Dr Masahiko Saito (Hiroshima University) and Dr Tomoyuki Koganezawa (JASRI) for the measurement of GIWAXS images, Prof. Koichi Mitsudo and Prof. Seiji Suga (Okayama University) for the CV measurements, and Prof. Naoshi Ikeda (Okayama University) for the AFM images, and Prof. Yoshihiro Kubozono (Okayama University) for the EQE and thickness measurement, and Ms Megumi Kosaka and Mr Motonari Kobayashi at the Department of Instrumental Analysis, Advanced Science Research Center, Okayama University, for the measurements of elemental analyses and the SC-NMR Laboratory of Okayama University for the NMR spectral measurements.

References

1 S. Holliday, J. E. Donaghey and I. McCulloch, *Chem. Mater.*, 2014, **26**, 647–663.
2 Y. He, W. Hong and Y. Li, *J. Mater. Chem. C*, 2014, **2**, 8651–8661.
3 H. Zhou, L. Yang and W. You, *Macromolecules*, 2012, **45**, 607–632.
4 L. Lu, T. Zheng, Q. Wu, A. M. Schneider, D. Zhao and L. Yu, *Chem. Rev.*, 2015, **115**, 12666–12731.
5 Y. Cai, L. Huo and Y. Sun, *Adv. Mater.*, 2017, **29**, 1605437.
6 H. N. Tsao, D. M. Cho, I. Park, M. R. Hansen, A. Mavrinskiy, D. Y. Yoon, R. Graf, W. Pisula, H. W. Spiess and K. Müllen, *J. Am. Chem. Soc.*, 2011, **133**, 2605–2612.
7 I. Kang, H.-J. Yun, D. S. Chung, S.-K. Kwon and Y.-H. Kim, *J. Am. Chem. Soc.*, 2013, **135**, 14896–14899.
8 H.-R. Tseng, H. Phan, C. Luo, M. Wang, L. A. Perez, S. N. Patel, L. Ying, E. J. Kramer, T.-Q. Nguyen, G. C. Bazan and A. J. Heeger, *Adv. Mater.*, 2014, **26**, 2993–2998.
9 G. Kim, S.-J. Kang, G. K. Dutta, Y.-K. Han, T. J. Shin, Y.-Y. Noh and C. Yang, *J. Am. Chem. Soc.*, 2014, **136**, 9477–9483.
10 S. Yum, T. K. An, X. Wang, W. Lee, M. A. Uddin and Y. J. Kim, *Chem. Mater.*, 2014, **26**, 2147–2154.
11 T. Lei, X. Xia, J.-Y. Wang, C.-J. Liu and J. Pei, *J. Am. Chem. Soc.*, 2014, **136**, 2135–2141.
12 Q. Wan, X. Guo, Z. Wang, W. Li, B. Guo, W. Ma, M. Zhang and Y. Li, *Adv. Funct. Mater.*, 2016, **26**, 6635–6640.
13 V. Vohra, K. Kawashima, T. Kakara, T. Koganezawa, I. Osaka, K. Takimiya and H. Murata, *Nat. Photonics*, 2015, **9**, 403–409.
14 Z. Li, D. Yang, X. Zhao, T. Zhang, J. Zhang and X. Yang, *Adv. Funct. Mater.*, 2018, **28**, 1705257.
15 J. Zhao, Y. Li, G. Yang, K. Jiang, H. Lin, H. Ade, W. Ma and H. Yan, *Nat. Energy*, 2016, **1**, 15027.
16 W. Zhao, D. Qian, S. Zhang, S. Li, O. Inganäs, F. Gao and J. Hou, *Adv. Mater.*, 2016, **28**, 4734–4739.

17 S. Li, L. Ye, W. Zhao, H. Yan, B. Yang, D. Liu, W. Li, H. Ade and J. Hou, *J. Am. Chem. Soc.*, 2018, **140**, 7159–7167.
18 Z. Yi, S. Wang and Y. Liu, *Adv. Mater.*, 2015, **27**, 3589–3606.
19 H. Choi, S.-J. Ko, T. Kim, P.-O. Morin, B. Walker, B. H. Lee, M. Leclerc, J. Y. Kim and A. J. Heeger, *Adv. Mater.*, 2015, **27**, 3318–3324.
20 H. Mori, M. Suetsugu, S. Nishinaga, N.-H. Chang, H. Nonobe, Y. Okuda and Y. Nishihara, *J. Polym. Sci., Part A: Polym. Chem.*, 2015, **53**, 709–718.
21 E. Wang, W. Mammo and M. R. Andersson, *Adv. Mater.*, 2014, **26**, 1801–1826.
22 S.-F. Liao, C.-T. Chen and C.-Y. Chao, *ACS Macro Lett.*, 2017, **6**, 969–974.
23 S. Nishinaga, H. Mori and Y. Nishihara, *Macromolecules*, 2015, **48**, 2875–2885.
24 H. Mori, S. Hara, S. Nishinaga and Y. Nishihara, *Macromolecules*, 2017, **50**, 4639–4648.
25 X. Guo, A. Facchetti and T. J. Marks, *Chem. Rev.*, 2014, **114**, 8943–9021.
26 H. Yan, Z. Chen, Y. Zheng, C. Newman, J. R. Quinn, F. Döts, M. Kastler and A. Facchetti, *Nature*, 2009, **457**, 679–687.
27 B. Fan, L. Ying, P. Zhu, F. Pan, F. Liu, J. Chen, F. Huang and Y. Cao, *Adv. Mater.*, 2017, **29**, 1703906.
28 I. Osaka and K. Takimiya, *Adv. Mater.*, 2017, **29**, 1605218.
29 C. Dou, X. Long, Z. Ding, Z. Xie, J. Liu and L. Wang, *Angew. Chem., Int. Ed.*, 2016, **55**, 1436–1440.
30 X. Long, Z. Ding, C. Dou, J. Zhang, J. Liu and L. Wang, *Adv. Mater.*, 2016, **28**, 6504–6508.
31 X. Long, Y. Gao, H. Tian, C. Dou, D. Yan, Y. Geng, J. Liu and L. Wang, *Chem. Commun.*, 2017, **53**, 1649–1652.
32 H. Zhou, L. Yang, A. C. Stuart, S. C. Price, S. Liu and W. You, *Angew. Chem., Int. Ed.*, 2011, **50**, 2995–2998.
33 Z. Chen, P. Cai, J. Chen, X. Liu, L. Zhang, L. Lan, J. Peng, Y. Ma and Y. Cao, *Adv. Mater.*, 2014, **26**, 2586–2591.
34 X. Liu, L. Nian, K. Gao, L. Zhang, L. Qing, Z. Wang, L. Ying, Z. Xie, Y. Ma, Y. Cao, F. Liu and J. Chen, *J. Mater. Chem. A*, 2017, **5**, 12619–17631.
35 T. L. Nguyen, H. Choi, S.-J. Ko, M. A. Uddin, B. Walker, S. Yum, J.-E. Jeong, M. H. Yun, T. J. Shin, S. Hwang, J. Y. Kim and H. Y. Woo, *Energy Environ. Sci.*, 2014, **7**, 3040–3051.
36 J. You, L. Dou, K. Yoshimura, T. Kato, K. Ohya, T. Moriarty, K. Emery, C.-C. Chen, J. Gao, G. Li and Y. Yang, *Nat. Commun.*, 2013, **4**, 1446.
37 N. Wang, Z. Chen, W. Wei and Z. Jiang, *J. Am. Chem. Soc.*, 2013, **135**, 17060–17068.
38 H. Mori, H. Nonobe and Y. Nishihara, *Polym. Chem.*, 2016, **7**, 1549–1558.
39 H. Mori, R. Takahashi, K. Hyodo, S. Nishinaga, Y. Sawanaka and Y. Nishihara, *Macromolecules*, 2018, **51**, 1357–1369.
40 Q. Liao, Y. Wang, M. A. Uddin, J. Chen, H. Guo, S. Shi, Y. Wang, H. Y. Woo and X. Duo, *ACS Macro Lett.*, 2018, **7**, 519–524.
41 M. A. Uddin, T. H. Lee, S. Xu, S. Y. Park, T. Kim, S. Song, T. L. Nguyen, S.-J. Ko, S. Hwang, J. Y. Kim and H. Y. Woo, *Chem. Mater.*, 2015, **27**, 5997–6007.
42 H. Huang, L. Yang, A. Facchetti and T. J. Marks, *Chem. Rev.*, 2017, **117**, 10291–10318.
43 Y. Liu, J. Zhao, Z. Li, C. Mu, W. Ma, H. Hu, K. Jiang, H. Lin, H. Ade and H. Yan, *Nat. Commun.*, 2014, **5**, 5293.
44 C.-Y. He, C.-Z. Wu, Y.-L. Zhu and X. Zhang, *Chem. Sci.*, 2014, **5**, 1317–1321.
45 H. Hu, K. Jiang, G. Yang, J. Liu, Z. Li, H. Lin, Y. Liu, J. Zhao, J. Zhang, F. Huang, Y. Qu, W. Ma and H. Yan, *J. Am. Chem. Soc.*, 2015, **137**, 14149–14157.
46 Q. Wu, S. Ren, M. Wang, X. Qiao, H. Li, X. Gao, X. Yang and D. Zhu, *Adv. Funct. Mater.*, 2013, **23**, 2277–2284.
47 J. Qi, X. Zhou, D. Yang, W. Qiao, D. Ma and Z.-Y. Wang, *Adv. Funct. Mater.*, 2014, **24**, 7605–7612.
48 B. C. Thompson, B. J. Kim, D. F. Kavulak, K. Sivula, C. Mauldin and J. M. J. Fréchet, *Macromolecules*, 2007, **40**, 7425–7428.
49 S. Subramaniyan, H. Xin, F. S. Kim and S. A. Jenekhe, *Macromolecules*, 2011, **44**, 6245–6248.
50 M. J. Frisch, G. W. Trucks, H. B. Schlegel, G. E. Scuseria, M. A. Robb, J. R. Cheeseman, G. Scalmani, V. Barone, B. Mennucci, G. A. Petersson, H. Nakatsuji, M. Caricato, X. Li, H. P. Hratchian, A. F. Izmaylov, J. Bloino, G. Zheng, J. L. Sonnenberg, M. Hada, M. Ehara, K. Toyota, R. Fukuda, J. Hasegawa, M. Ishida, T. Nakajima, Y. Honda, O. Kitao, H. Nakai, T. Vreven, J. A. Montgomery, J. E. Peralta, F. Ogliaro, M. Bearpark, J. J. Heyd, E. Brothers, K. N. Kudin, V. N. Staroverov, T. Keith, R. Kobayashi, J. Normand, K. Raghavachari, A. Rendell, J. C. Burant, S. S. Iyengar, J. Tomasi, M. Cossi, N. Rega, N. J. Millam, M. Klene, J. E. Knox, J. B. Cross, V. Bakken, C. Adamo, J. Jaramillo, R. Gomperts, R. E. Stratmann, O. Yazyev, A. J. Austin, R. Cammi, C. Pomelli, J. W. Ochterski, R. L. Martin, K. Morokuma, V. G. Zakrzewski, G. A. Voth, P. Salvador, J. J. Dannenberg, S. Dapprich, A. D. Daniels, Ö. Farkas, J. B. Foresman, J. V. Ortiz, J. Cioslowski and D. J. Fox, *Gaussian 09, Revision D. 01*, Gaussian, Inc., Wallingford, CT, 2013.
51 Y. Sun, J. H. Seo, C. J. Takacs, J. Seifter and A. J. Heeger, *Adv. Mater.*, 2011, **23**, 1679–1683.
52 V. Shrotriya, Y. Yao, G. Li and Y. Yang, *Appl. Phys. Lett.*, 2006, **89**, 063505/1–3.
53 C.-Y. He, S. Fan and X. Zhang, *J. Am. Chem. Soc.*, 2010, **132**, 12850–12852.
54 X. Zhang, S. Fan, C.-Y. He, X. Wan, Q.-Q. Min, J. Yang and Z.-X. Jiang, *J. Am. Chem. Soc.*, 2010, **132**, 4506–4507.
55 P. Cai, Z. Chen, L. Zhang, J. Chen and Y. Cao, *J. Mater. Chem. C*, 2017, **5**, 2786–2793.
56 I. Osaka, M. Shimawaki, H. Mori, I. Doi, E. Miyazaki, T. Koganezawa and K. Takimiya, *J. Am. Chem. Soc.*, 2012, **134**, 3498–3507.
57 A. C. Stuart, J. R. Tumbleston, H. Zhou, W. Li, S. Liu, H. Ade and W. You, *J. Am. Chem. Soc.*, 2013, **135**, 1806–1815.
58 K. Takimiya, I. Osaka and M. Nakano, *Chem. Mater.*, 2014, **26**, 587–593.

59 X. Jiang, Y. Yang, J. Zhu, T.-K. Lau, P. Cheng, X. Lu, X. Zhan and X. Chen, *J. Mater. Chem. C*, 2017, **26**, 8179–8186.
60 G. P. Kini, W. S. Lee, W. S. Shin, S.-J. Moon, C. E. Song and J.-C. Lee, *J. Mater. Chem. A*, 2016, **4**, 18585–18597.
61 C.-C. Ho, C.-A. Chen, C. Y. Chang and W.-F. Darling Su, *J. Mater. Chem. A*, 2016, **4**, 18585–18597.
62 W. Tress, A. Petrich, M. Hummert, M. Hein, C. Leo and M. Riede, *Appl. Phys. Lett.*, 2011, **98**, 063301.
63 Y. Huang, E. J. Kramer, A. J. Heeger and G. C. Bazan, *Chem. Rev.*, 2014, **114**, 7006–7043.
64 L. Ye, B. A. Collins, X. Jiao, J. Zhao, H. Yan and H. Ade, *Adv. Energy Mater.*, 2018, **8**, 1703058.

